

## Porosity and Pt content in the catalyst layer of PEMFC: effects on diffusion and polarization characteristics

Ai Suzuki<sup>1,\*</sup>, Tatsuya Hattori<sup>2</sup>, Ryuji Miura<sup>2</sup>, Hideyuki Tsuboi<sup>2</sup>, Nozomu Hatakeyama<sup>2</sup>, Hiromitsu Takaba<sup>2</sup>, Mark C. Williams<sup>1</sup>, and Akira Miyamoto<sup>1,2</sup>

<sup>1</sup>New Industry Creation Hatchery Center, Tohoku University, Sendai 980-8579, Japan

<sup>2</sup>Graduate School of Engineering, Tohoku University, Sendai 980-8579, Japan

\*E-mail: [ai@aki.che.tohoku.ac.jp](mailto:ai@aki.che.tohoku.ac.jp)

Received: 21 September 2010 / Accepted: 15 October 2010 / Published: 1 December 2010

---

A three-dimensional (3-D) pore network model of polymer electrolyte membrane fuel cell (PEMFC) is presented in order to evaluate the effect of pore size and the effective diffusion coefficient in random porous media. The model of pseudo cathode catalyst layer (CCL) consists of pores and a random distribution of carbon supported platinum (Pt/C) and electrolytes, which were generated on a computer by means of Monte Carlo method. In this study, we utilized this 3-D meso-scale porous model of the CCL, and investigated tortuosity of pores, electrolyte connectivity. The effective Knudsen diffusion coefficient can be successfully obtained. This meso-scale model is applied to study the effects of porosity, pore size and Pt content on the polarization characteristics of the PEMFC. The relation between the composition of the CCL and the characteristics of polarization curve has been clarified.

---

**Keywords:** Catalyst layer, pore network, 3-D, tortuosity, effective diffusion coefficient, Pt/C, electrolytes, Knudsen diffusion

### 1. INTRODUCTION

The polymer electrolyte membrane fuel cell (PEMFC) is considered to be a promising power source for stationary and automotive applications. The cathodic overpotential caused by the cathodic half-reaction, i.e. the oxygen reduction reaction (ORR) is given by



In this reaction, however, the polarization loss in the cathodes accounts for 80 % of the total

loss (1). Therefore, the performance of a PEMFC is limited by the ORR on the cathode side. Moreover, the mass transport losses caused by the diffusion of gaseous oxygen through the porous electrode and the diffusion of dissolved oxygen to the reaction side determine the performance. To guarantee the durability of cell performance essential for long-term, stable operation, the polarization loss of the PEMFC must be overcome. However, real-time experimental verification of PEMFC durability takes considerable time and effort. Therefore, the theoretical prediction of the polarization characteristics is desirable as an alternative method to experimental durability examinations.

It is already known that the polarization curves depend on the mass ratio of the electrolyte in the catalyst layer, and the relation between the structure and composition of a catalyst layer and the cell performance have been clarified both experimental and theoretical means. Moreover, operating conditions, including the oxygen partial pressure, temperature and humidity affect cell performances. V. D. Diwakar and V. R. Subramanian gave analytical solutions for the electrolyte loading distribution (2). Although various two-phase models (2,3,4), 3-D models (5,6) and lumped model (7) have been proposed for the analysis of a PEMFC, the relationship between the pore networks in the cathode catalyst layer (CCL) and the polarization characteristics has not been adequately considered. Hence the meso-scale three-dimensional porous structure of the CCL was designed, and then, the electrocatalytic reaction, proton conductivity, and the characteristics of polarization loss were investigated.

## 2. METHODS

### 2.1. Modeling of cathode catalyst layer

The model considered the cathode side of a PEMFC; the losses on the anode side were neglected because of the low amount of polarization of the hydrogen electrode. The inner structure of the porous gas diffusion electrode was taken into account. In the catalyst layer, the dispersed catalyst (Pt/C) forms agglomerates filled with the electrolyte. These domains were surrounded by channels through which the reactant gases can diffuse. Our former study corresponds to clarifying the influences of thickness of electrolytes on polarization curves (8).

In this review, we modeled a CCL which is a composite containing distributed Pt catalysts, carbon supports and they were intermixed with electrolytes. Nano-sized Pt particles were dispersed on carbon powder. The Pt is supported on the surface of carbon particles. The weights percent of Pt, carbon and PEM varies spatially in the catalyst layer. The ratio of carbon, electrolyte, Pt and pores can be considered along the direction of the gas diffusion layer (GDL) to the polymer electrolyte membrane (PEM). The sum of the electrolyte volume fraction, the pore space volume fraction and the Pt dispersed carbon volume fraction is equal to 1 as shown in mass-balance eq. [2].

$$\varepsilon + \zeta + \gamma = 1 \quad [2]$$

The volume fraction of the electrolyte,  $\zeta$  was obtained with the following process. The weight of the electrolyte was calculated from the electrolyte/carbon (E/C) weight ratio. The volume of the

electrolyte was then estimated from its weight and density. We also investigated a quantitative characterization of the microstructure of the catalyst layers, in particular, the electrolyte coverage and thickness.  $\gamma$  is the carbon and catalyst volume fraction and determined from eq. [3]:

$$\gamma = \left( \frac{1}{\rho_{Pt}} + \frac{1 - \%Pt}{\%Pt \cdot \rho_C} \right) \frac{m_{Pt}}{L} \quad [3]$$

where  $\rho_{Pt}$  and  $\rho_C$  are the mass densities of the Pt and carbon black and  $\%Pt$  is the mass percentage of Pt supported on the carbon black. It should be noted that the pore fraction  $\varepsilon$  and the Pt dispersed carbon fraction  $\gamma$  are related to the four parameters ( $\%Pt$ ,  $m_{Pt}$ ,  $L$  and  $\zeta$ ). Therefore, for a given active layer, only the four parameters ( $\%Pt$ ,  $m_{Pt}$ ,  $L$  and  $\zeta$ ) need to be specified.

The schematic diagram of three-dimensional modeling regions and modeling procedures of CCL are shown in Fig.1.

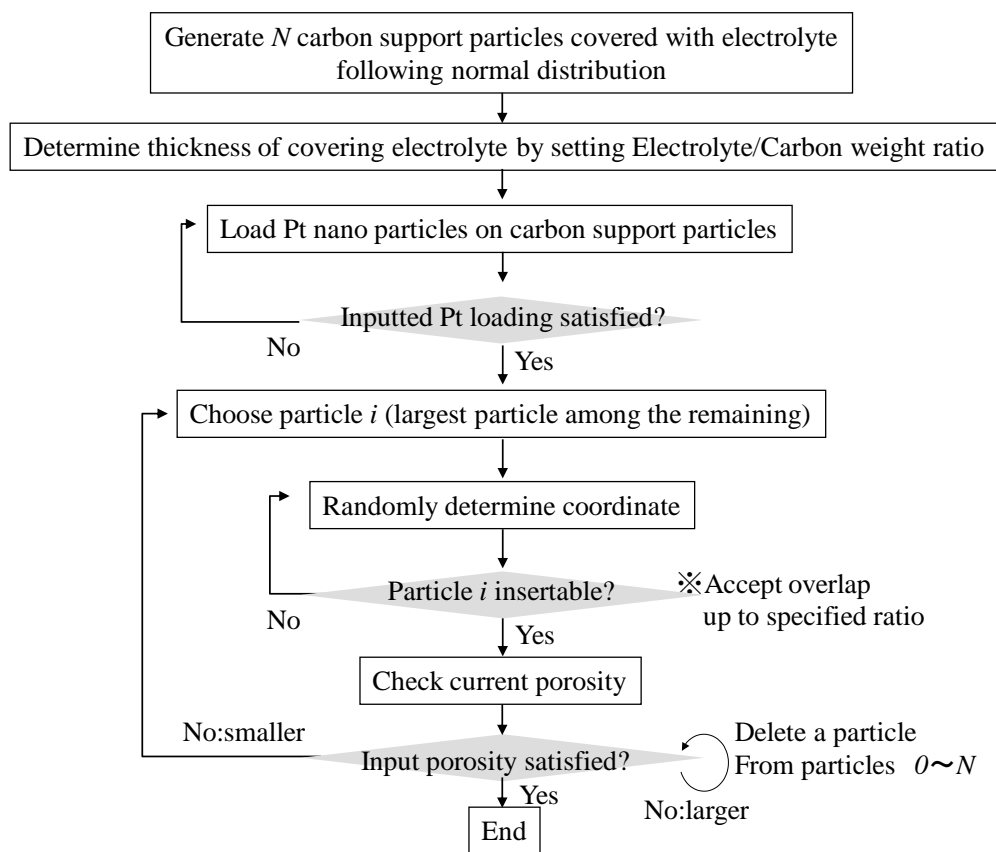


**Figure 1.** Algorithm for constructing a three-dimensional cathode catalyst layer mode

The original software, *dendenFC*® enabled this modeling technique and solving a series of mass transport and electrochemical equations. Figure 2(a) shows the constructed 3-D catalyst layer model. Here, the catalyst layer contains three phases, the gas phase, mixed Pt/C and the electrolyte

phase. On the bottom boundary, protons migrate into CCL from the membrane. On the upper boundary, oxygen and electrons transport into the layer through the GDL. In the present study, the range of the catalyst layer, which is considered typically to range from 10 μm to 20 μm thick, was set at 11 μm.

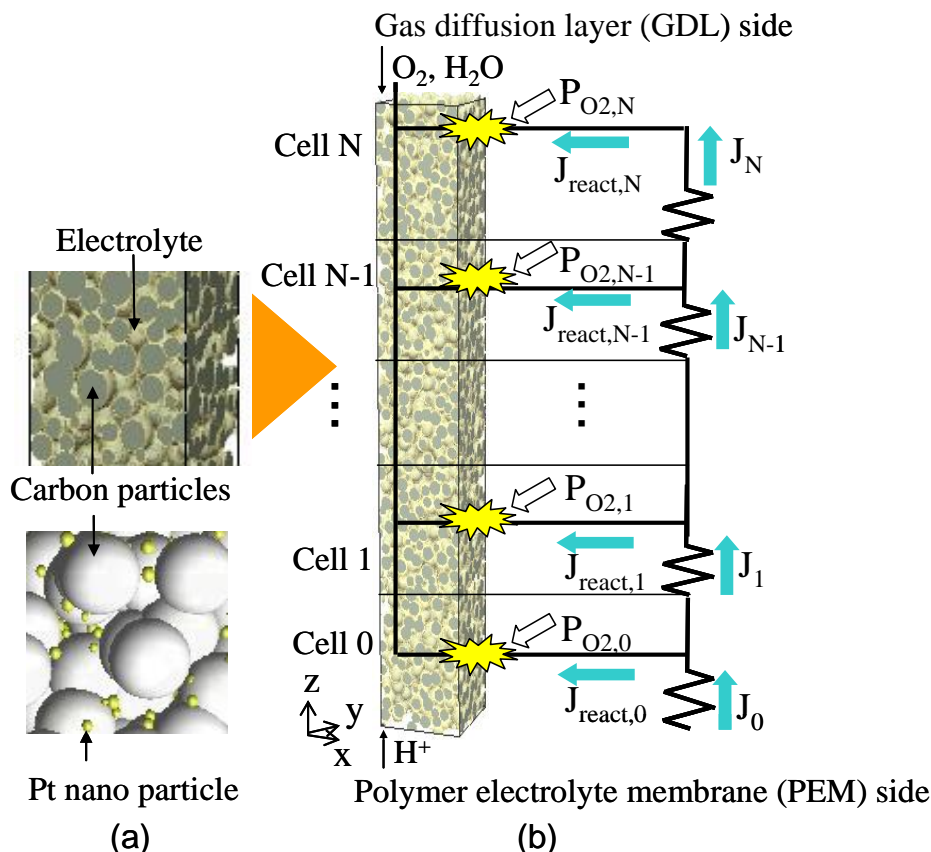


**Figure 2.** (a) A constructed 3-D model of porous cathode catalyst layer composite containing distributed Pt/C catalyst intermixed with electrolyte (b) Solution scheme for the overpotential of PEMFC

### 2.2. Tortuosity of gas in pore network

The tortuosity,  $\tau$  of a pore network is the result of the merging, branching, and curving of pores. These connected pores form continuous paths for gas flow. Tortuosity is here defined as the ratio of the average path of gas flow in free space,  $L_f$ , to the length of that in the catalyst layer,  $L_c$ .

$$\tau = L_c / L_f \quad [4]$$

In computation of the mean tortuosity of 3-D pore network, we consider a unit cell. The computation procedure for the pore tortuosity was based on a Monte Carlo method and is illustrated in Fig. 3, which is calculated based on the Monte Carlo method. In the case where each cell was  $1.0 \times 1.0 \times 11.0 \mu m$ , the constructed CCL model was finely divided into  $100.0 \times 100.0 \times 1100.0$  meshes in the

x-, y-, and z-directions, respectively. Each of these divided meshes was classified as corresponding to a pore, carbon, or electrolyte by judging whether the center of the mesh was a pore, carbon, or electrolyte. Actually computed tortuosity,  $\tau$  of two kinds of different porous CCL was summarized in Table 2.

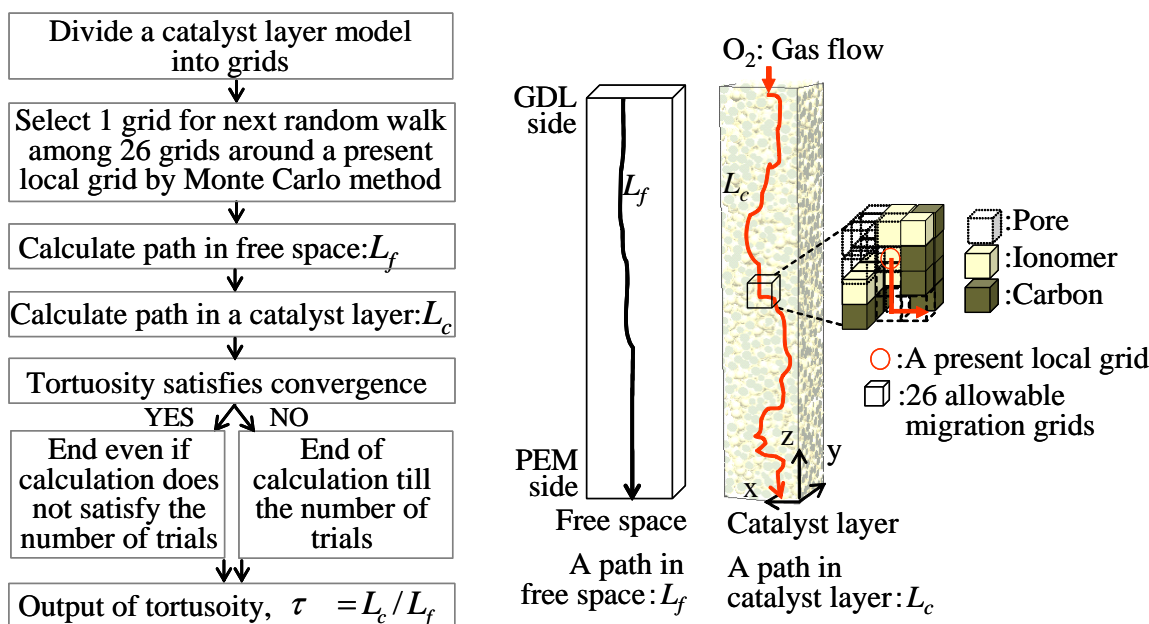


**Figure 3.** Computation procedure for tortuosity by Monte Carlo method

### 2.3. Gas diffusion coefficient

The constructed model took into account the mass-transport phenomena caused by multicomponent gas diffusion through the CCL. The oxygen flux,  $N_{O_2}$ , through the catalyst layer was assumed to be driven by a concentration gradient. It was thus determined by Fick’s law for the diffusion of the gas, which can be described as follows;

$$\frac{dc_{O_2}}{dx} = -\frac{N_{O_2}}{D_{O_2}^{eff}} \quad [5]$$

Here,  $c_{O_2}$  represents the oxygen concentration, which can be expressed as follows by considering molecular diffusion and Knudsen diffusion (9, 10).  $D_{O_2}^{eff}$  is the effective oxygen gas diffusion in the CCL, corrected for the porosity  $\varepsilon$  and the tortuosity  $\tau$  of the CCL, and is related to the Knudsen diffusion coefficients,  $D_{kn}$  and  $D_{O_2}$ .

$$D_{O_2}^{eff} = \frac{\varepsilon}{\tau} \frac{1}{1/D_{O_2} + 1/D_{kn}} \quad [6]$$

$D_{O_2}$  is the molecular diffusion coefficient ( $\text{cm}^2 \text{s}^{-1}$ ) of  $\text{O}_2$  in the pores.  $D_{kn}$  is the Knudsen diffusion coefficient ( $\text{cm}^2 \text{s}^{-1}$ ) for the porous structure, in which  $d_p$  ( $\mu\text{m}$ ) is the average pore diameter. Because the Knudsen effect is dependent on the temperature and molecular weight, we used temperature,  $T = 353 \text{ K}$  ( $80 \text{ }^\circ\text{C}$ ) and oxygen molecular weight,  $M_{O_2} = 32 \text{ kg kmol}^{-1}$ . The value of  $d_p$  was the size of local pore diameter as shown in Fig. 4, which was calculated by scanning a CCL structure. Computed  $d_p$  is reflected in eq.[7].

$$D_{kn} = \frac{d_p}{3} \langle v \rangle = \frac{d_p}{3} \sqrt{\frac{8RT}{\pi M_{O_2}}} \quad [7]$$

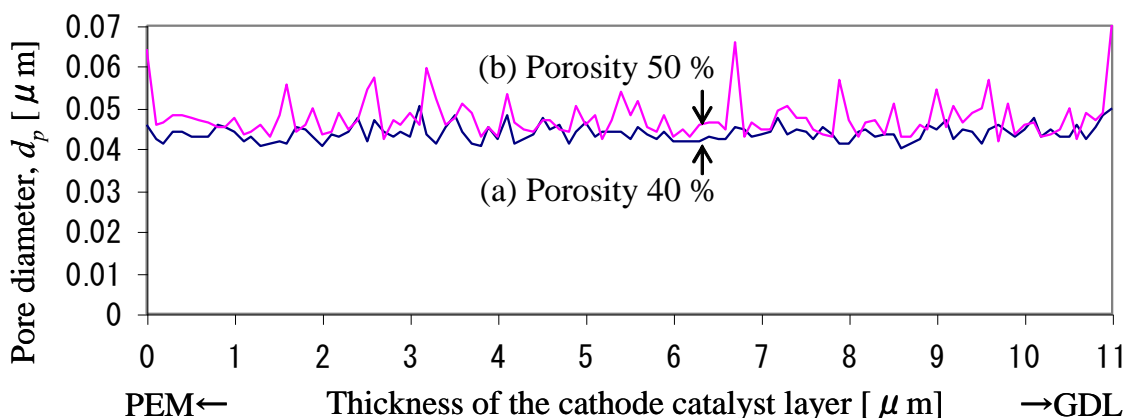


**Figure 4.** Average pore diameter of cathode catalyst layer that reflect the diffusion coefficient (a) Porosity 40%, Electrolyte 20wt%, Pt 10wt% (b) Porosity 50%, Electrolyte 20wt%, Pt 10wt%

In the case of the effective diffusion coefficient in GDL,  $D_{eff}$  used to account for oxygen gas diffusion, has been modified by the commonly employed Bruggemann relation (11) through the void region of the GDL and a correction factor to account for the non-diffusing space occupied by the solid fragments.

$$\text{In GDL, } D_{eff,O_2} = D_{O_2} \varepsilon_{GDL}^{1.5} \quad [8]$$

Here,  $\varepsilon_{GDL}$  is the porosity of the GDL, and this value is shown in Table 1.

#### 2.4. ORR and Henry's constant

Fig. 2(b) shows the solution scheme for the overpotential. Numerical simulations were carried out for the fuel cell operation with the conventional flow field and on the gas flow. The ORR kinetics follows Tafel's law and the oxygen concentration, as shown by the following eq.[9].

$$i_{r,i} = i_0 \left\{ \frac{C_{O_2}^{dis,i}}{C_{O_2}^{ref}} \exp\left(\alpha_c \frac{nF}{RT} \eta_i\right) - \exp\left((\alpha_c - 1) \frac{nF}{RT} \eta_i\right) \right\} \quad [9]$$

where  $C_{O_2}^{ref}$  is the reference oxygen concentration (12), and the value is shown in Table 3.  $i_0$  is the reference exchange current density,  $\alpha_c$  is the cathode charge transfer coefficient and  $\eta_i$  is the electrode activation overpotential.  $C_{O_2}^{dis,i}$  is the dissolved oxygen concentration in the electrolyte, determined by Henry's law.

$$C_{O_2}^{dis,i} = \frac{C_{O_2}}{K_{O_2}} = \frac{P_{O_2}}{RTK_{O_2}} \quad [10]$$

The dissolved oxygen concentration at the gas/electrolyte interface is determined from the solubility of oxygen using the Henry's law.  $K_{O_2}$  is the Henry's constant (13) for the oxygen gas dissolution in the electrolyte. The Henry law constant for oxygen,  $K_{O_2}$  is calculated from the following empirical relation.

$$K_{O_2} = \frac{1}{RT} \exp\left(-\frac{666}{T} + 14.1\right) \quad [11]$$

The experimental data of Parthasarathy et al. was used to correlate the reference exchange current density for ORR on the Pt-electrolyte interface with temperature in the following expression (14, 15),

$$\log_{10}(i^0) = 3.507 - \frac{4001}{T} \quad [12]$$

The open circuit potential (16) is as follows;

$$V_0 = 1.23 - 9.0 \times 10^{-4} (T - 298.15) \quad [13]$$

## 2.5. Proton conductivity

The proton conductivity of Nafion as a function of the water content and temperature has been reported by Springer and Zawodinski (17) and is expressed by the following experimental equation.

$$\sigma = (0.005139\lambda - 0.00326) \exp\left[1268\left(\frac{1}{303} - \frac{1}{T}\right)\right] \quad [14]$$

The relative humidity was used to determine the local water content in the electrolyte phase (18),  $\lambda$ .

$$\lambda = 0.3 + 10.8RH - 16RH^2 + 14.1RH^3 \quad [15]$$

$$\begin{aligned} \lambda &= 0.043 + 17.81a - 39.85a^2 + 36.0a^3 \quad \text{at } (a < 1) \\ &= 14.0 + 1.4(a-1) \quad \text{at } (1 \leq a \leq 3) \end{aligned} \quad [16]$$

$$a = \frac{P_{\text{vaporH}_2\text{O}}}{P_{\text{sat}}} \quad [17]$$

where  $a$  is water vapor activity (ratio of the water vapor pressure and saturation pressure), and  $\lambda$  is the water content of electrolyte, which is related to the water vapor activity. The water vapor was fed until the relative pressure,  $p/p_{\text{sat}}$  ( $p_{\text{sat}}$ , saturated vapor pressure, 47 kPa at 80°C). The saturation pressure,  $p_{\text{sat}}$  (Pa) can be expressed in terms of the local temperature (17).

$$\log_{10}(p/p_{\text{sat}}) = -2.1794 + 0.02953(T-273) - 9.1837 \times 10^{-5}(T-273)^2 + 1.4454 \times 10^{-7}(T-273)^3 \quad [18]$$

The coupled set of equations was solved iteratively, and the solution was considered to be convergent when the relative error in each field between two consecutive iterations was less than 0.05. Because the electrode is very thin and its electronic conductivity is sufficiently high, the electronic phase potential is assumed to be uniform (19). Thus the electron transport does not need to be considered. Under this assumption, the mixed phase is treated as the electrolyte phase and the ionic conductivity is duly corrected with respect to the mixed phase volume fraction using Bruggeman correlation as follows (19):

$$\sigma^{\text{eff}} = \sigma_0 \varepsilon_{\text{ion}}^{1.5} \quad [19]$$

## 2.6. Solving electrochemical reaction scheme

The following assumptions are made to solve the electrochemical reaction scheme:

1. Isothermal and steady-state operation.
2. Uniform temperature throughout the electrode.
3. Diffusion of O<sub>2</sub> in the electrolytes and internal pores.
4. Gas component (O<sub>2</sub> and H<sub>2</sub>O) sorption on the electrolyte
5. The electrochemical reaction in the CCL occurs on the Pt active surface area.
6. Water in liquid form is produced as a result of the electrochemical reaction.
7. Water vapor can condense depending on the local partial pressure of the water vapor and its saturation pressure at the operating temperature.
8. Liquid water is assumed to exist in the form of small droplets, and its volume reduces the pore volume in the CCL.

### 3. RESULTS AND DISCUSSION

#### 3.1. 3-D CCL model with different porosity

The size of each cell was  $1.0 \times 1.0 \times 11.0 \mu\text{m}$ , and the thickness of a CCL was  $L = 11.0 \mu\text{m}$ , with different porosity, 40 % and 50 %. The cell was assumed to be fed by air ( $C_{in}^{N_2} / C_{in}^{O_2} = 0.79/0.21$  on the cathode side). Constructed models contained the same Pt loading, 10 wt% and the carbon particles with electrolytes but they have different porosity, 40 % and 50 %. Structural parameters for the GDL are summarized in Table 1. Structural parameters for the CCL are summarized in Table 2.

**Table 1.** Structural parameters for the GDL

GDL structural data	Numerical value
Porosity $\varepsilon_{GDL}$ [-]	0.4
Thickness, $L_{GDL}$ [ $\mu\text{m}$ ]	370
Average pore diameter [nm]	$1.0 \times 10^4$

**Table 2.** Structural parameters for the CCL

CCL structural data	Numerical value
Diameter of Pt [nm]	3.0
Catalyst layer thickness, $L_{CCL}$ [ $\mu\text{m}$ ]	11
Computed tortuosity, $\tau$ [-]	1.13 (Porosity 40 %) 1.09 (Porosity 50 %)

#### 3.2. Component ratio of CCL and active Pt surface area

These two CCL models were finely divided into  $100.0 \times 100.0 \times 1100.0$  meshes in the x-, y- and z-directions, respectively and we analyzed the sectional component ratio and Pt surface area of two types of CCL models. Fig. 5(a) corresponds to the section of CCL with porosity 40%, electrolyte 20wt% and Pt 10wt%. Fig. 5(b) corresponds to the section of the other CCL with porosity 50 %, electrolyte 20 wt% and Pt 10 wt%. Active Pt surface area on the CCL of the porosity 40 % shows broader than that of porosity 50 %.

#### 3.3. Relation of porosity in CCL and polarization characteristics

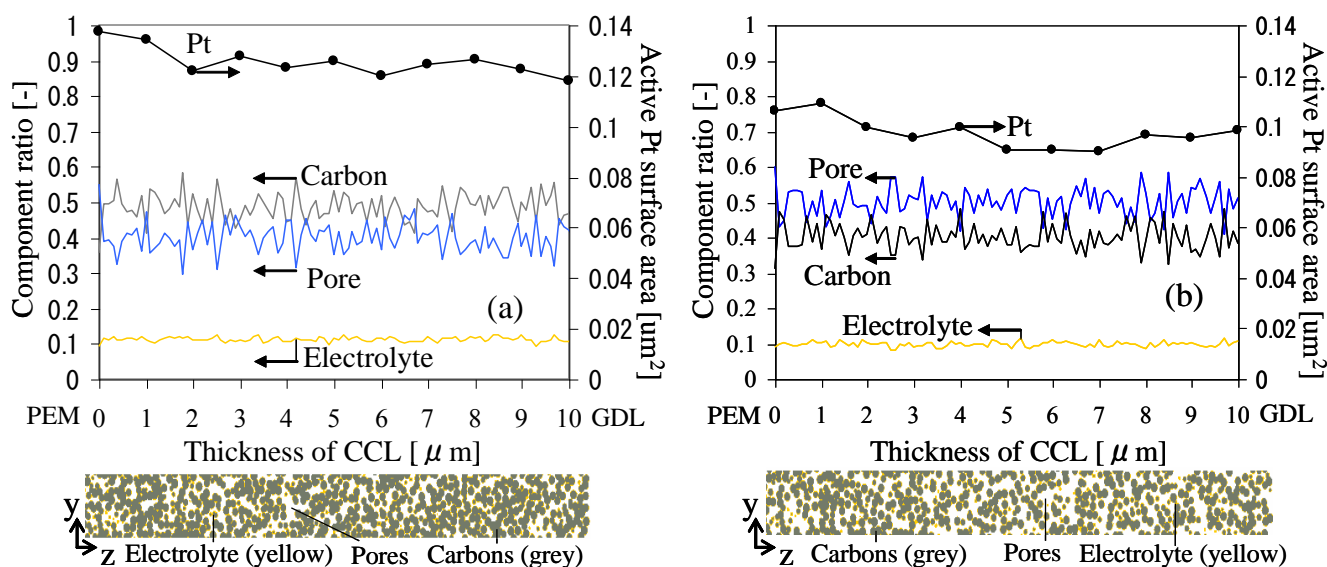
It should be noted that the term “polarization curve” refers to the voltage loss versus current density curve throughout this article instead of the standard I-V curve, otherwise used widely in fuel cell literature. The performance of polarization curve was simulated at  $80 \text{ }^\circ\text{C}$ , air as oxidizer, 1 atm as total pressure. Cell operating conditions are summarized in Table 3.

Fig.6 shows the effect of the different porosity on the polarization curves. The same Pt loading with 10 wt% Pt/C and electrolytes with 20wt% are contained in thickness of  $11.0 \mu\text{m}$  catalyst layer, with different porosity with 40 % and 50%. When oxygen transport becomes dominant as higher current densities, the performance of larger porosity, 50 % is considerable decrease of voltage loss due

to the enhanced oxygen transport. C. M. B. Rodriguez classified current-potential curve into four areas; a loss in tension generated by Redox reactions irreversibility developing on the active layer of the electrodes, activation losses, ohmic losses, and loss of dissemination in feeding of reactive gases (20). Especially, CCL containing larger porosity, 50 % leads to higher ohmic drop due to the presence of less contact phase to electrolyte volume fraction to conduct protons.

**Table 3.** Cell operating conditions

Cell operating condition	Numerical value
Cell temperature, $T$ [°C]	80
Atmospheric pressure, [Pa]	101,325
Pressure at the cathode gas channel inlet [atm]	1
Relative humidity of inlet fuel stream [%]	10
Inlet nitrogen/oxygen mole fraction ratio [-]	0.79/0.21
Open-circuit potential, $V_0$ [V]	1.18
Cathode charge transfer coefficient, $\alpha_c$ [-]	0.5
Faraday constant, $F$ [C mol <sup>-1</sup> ]	96487
Number of electrons, $n$ [-]	4
The reference concentration of oxygen, $C_{O_2}^{ref}$ [mol/m <sup>3</sup> ]	3.39



**Figure 5.** Component ratio and active Pt surface area of 2 types of cathode catalyst layer (CCL) models and section views in Y-Z direction  
 (a) Porosity 40%, Electrolyte 20wt%, Pt 10wt%      (b) Porosity 50%, Electrolyte 20wt%, Pt 10wt%

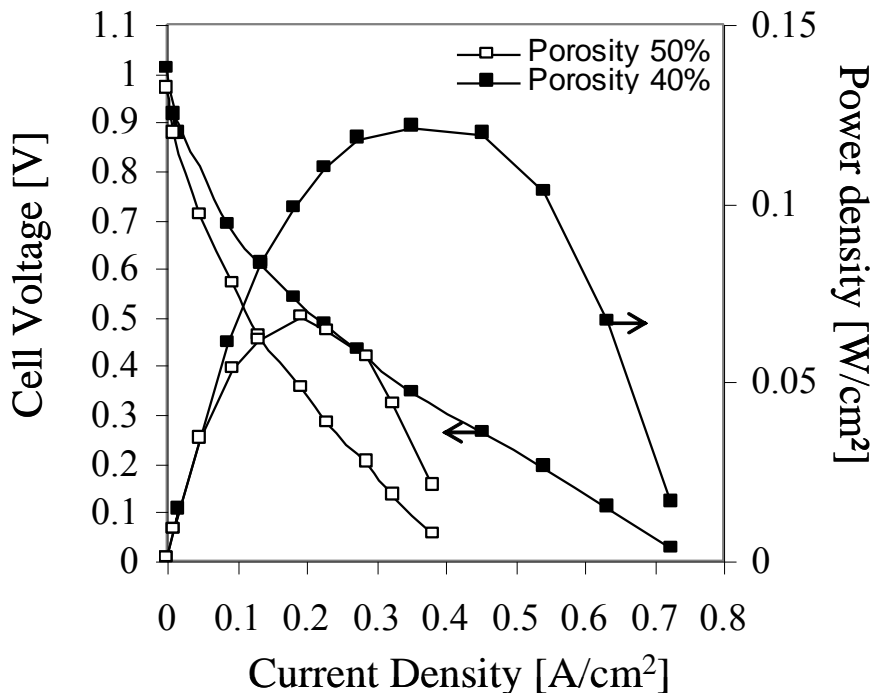


**Figure 6.** Effect of the different porosity on the polarization curves. 2 CCL contains same 10 wt% Pt/C and electrolytes 20wt% with different porosity with 40 % and 50%

3.4. Relation of Pt content in CCL and polarization characteristics

For comparing polarization curves of different loadings of Pt, 10 wt%, 30 wt% and 50 wt% on carbon supports in thickness of 11.0  $\mu\text{m}$  catalyst layer. We modeled three different Pt loading CCL structures with same porosity 40 % and electrolyte 20 w%. Active Pt surface areas in these three CCL models were shown in Fig.7.

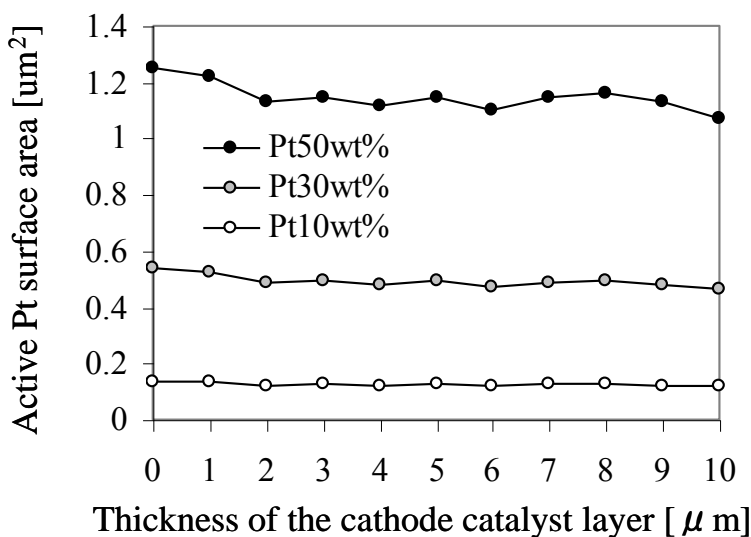


**Figure 7.** Active surface area of Pt in three CCL models with Porosity 40% and Electrolyte 20wt%.

It indicated that the active Pt surface area of 50 wt% Pt was the broadest among three kinds of CCL models. As a result, cell performances of three CCLs were shown in Fig. 8. The CCL containing 50 wt% Pt shows the highest performance among three CCL structures. When the porosity and content of electrolyte are same, the cell shows better performance as Pt active surface area became broader.

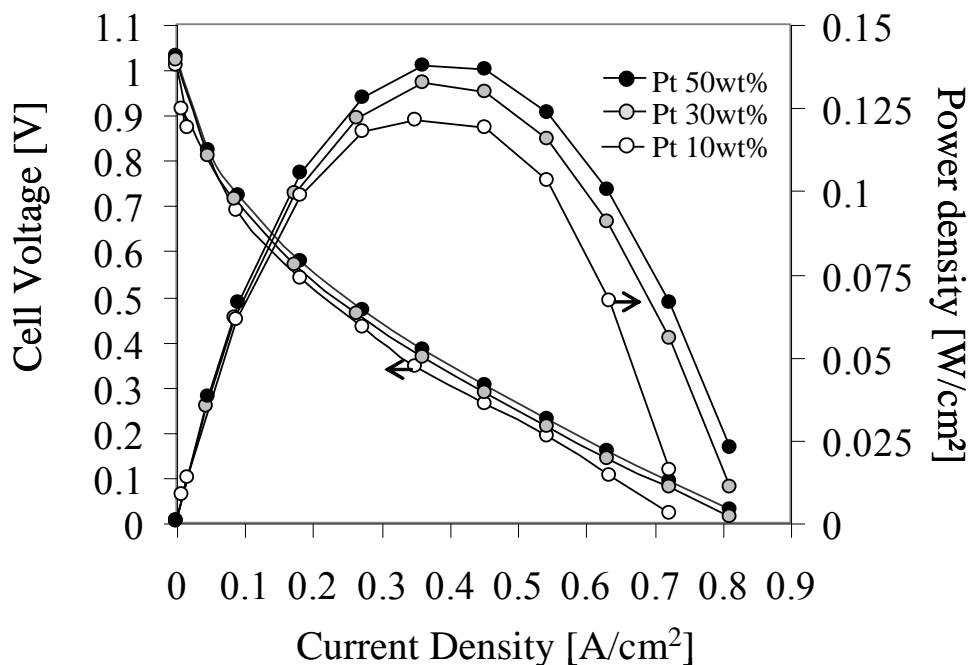


**Figure 8.** Effect of the different loading of Pt on the polarization curves in three CCL with porosity 40% and electrolyte 20wt%.

#### 4. CONCLUSIONS

We developed a three-dimensional modeling scheme for a CCL of PEMFC. The dependence of oxygen diffusion coefficient and proton conductivity on cathode performance has been investigated.

We modeled two kinds of CCLs which contains Pt loading of 10 wt% Pt/C and 20 wt% electrolytes with different porosity, 40% and 50 % in order to investigate the effect of porosity on the performance. As a result, the cell performance of 40 % porosity is better than that of 50% porosity.

Next, we modeled three kinds of CCLs which equally contains 40 % porosity and 20 wt% electrolyte in order to compare polarization curves of different loadings of Pt, 10 wt%, 30 wt% and 50 wt% on carbon supports. As a result, the cell performance of 50 wt% Pt is highest among three CCL structures are shown. In both studies, we performed the pore level analysis of oxygen transport through the systematic developed tools of a numerical simulation of CCL microstructure.

## 5. LIST OF SYMBOLS

$C_{O_2}^{ref}$	The oxygen reference concentration, $\text{molcm}^{-3}$
$C_{O_2}^{dis,i}$	The dissolved $O_2$ concentration of cell $i$ in the electrolyte, $\text{mol cm}^{-3}$
$D_{O_2}^{eff}$	The effective $O_2$ diffusion coefficient in the cell of $i$ , $\text{cm}^2\text{s}^{-1}$
$dPO_2$	The deviation in $O_2$ partial pressure (atm) between cell $i$ and cell $i + 1$
$dx$	The length in the direction of the thickness of the catalyst layer of each cell
$F$	Faraday's constant, $96485, \text{C mol}^{-1}$
$i$	The cell number
$i_{r,i}$	The reaction current density in the cell $i$ , $\text{Acm}^{-2}$
$i_0$	The exchange current density, $\text{Acm}^{-2}$
$K_{O_2}$	Henry's constant for oxygen dissolution in polymer electrolyte
$L_{CCL}$	The thickness of the cathode catalyst layer (CCL), $\mu\text{m}$
$L_{GDL}$	The thickness of the gas diffusion layer, $\mu\text{m}$
$m_{Pt}$	The catalyst mass loading per unit area of the cathode, $\text{gm}^{-2}$
$n$	The number of electrons transferred in the cathode reaction per $O_2$ molecule, 4, -
$N_{O_2,i}$	The $O_2$ flux, $\text{molcm}^{-2}\text{s}^{-1}$ into the cell $i$
%Pt	The mass percentage of Pt supported on the carbon
$\langle v \rangle$	The mean thermal velocity of molecules, $\text{m/s}$
$R$	Gas constant, $8.314, \text{J mol}^{-1}\text{K}^{-1}$
$T$	The cell temperature, $\text{K}$
$\tau_{pore}$	The tortuosity factor for the pores, -
$\alpha_c$	The cathode transfer coefficient, 0.5, -
$\varepsilon$	Porosity of the cathode catalyst layer (CCL), -
$\varepsilon_{GDL}$	Porosity of the GDL, -
$\gamma$	Volume fraction of carbon and Pt
$\zeta$	Electrolyte fraction in the active layer
$\eta_i$	The activation overpotential, $\text{V}$
$\lambda$	The water content, -
$\rho_{Pt}$	The density of platinum, $21.5 \times 10^3 \text{ mg/cm}^3$ (21)
$\rho_C$	The density of carbon, $2.0 \times 10^3 \text{ mg/cm}^3$ (21)
$\rho_{el}$	The density of electrolyte (Nafion), $1.9 \times 10^3 \text{ mg/cm}^3$ (21)
$\sigma$	The conductivity, $\text{S/cm}$
$\pi$	Circular constant, 3.14, -

## References

1. H. Inoue, E. Higuchi, Japanese patent 2009-252521.
2. V. D. Diwakar, V. R. Subramanian, *J. Electrochem. Soc.*, 152-5 (2005) A984.
3. A. Z. Weber, R. M. Darling, and J. Newman, *J. Electrochem. Soc.*, 151 (2004) A1715.
4. L. You and H. Liu, *Int. J. Heat Mass Transfer*, 45 (2002) 2277.
5. S. Mazumder and J. V. Cole, *J. Electrochem. Soc.*, 150 (2003) A1510.
6. T. Berning and N. Djilali, *J. Electrochem. Soc.*, 150 (2003) A1589.
7. M. Youssef, K. E. AL-NAdi, M. H. Khalil, *Int. J. Electrochem. Sci.*, 5 (2010) 267.
8. T. Hattori, A. Suzuki, R. Sahnoun, M. Koyama, H. Tsuboi, N. Hatakeyama, A. Endou, H. Takaba, M. Kubo, C. A. Del Carpio, A. Miyamoto, *Appl. Surf. Sci.*, 254 (2008) 7929.
9. W. Sun, B.A. Peppley, K. Karan, *Electrochim. Acta*, 50 (2005) 3359.

10. D. Song, Q. Wang, Z. Liu, T. Navessin, M. Eikerling, S. Holdcroft, *J. Power Sources*, 126 (2004) 104.
11. C. Boyer, S. Gamburgzev, O. Velez, S. Srinivasan, and A. J. Appleby, *Electrochim. Acta.*, 43 (1998) 3703.
12. P. T. Nguyen, T. Berning<sup>1</sup>, N. Djilali, *J. Power Sources.*, 130 (2004) 149.
13. J.J. Baschuk, X. Li, *J. Power Sources.*, 86 (2000) 181.
14. C. Marr, X. Li, *J. Power Sources.*, 77 (1999) 17.
15. A. Parthasarathy, S. Srinivasan, A. J. Appleby, C. R. Martin, *J. Electrochem. Soc.*, 139 (1992) 2530.
16. A. Vorobev, O. Zikanov, T. Shamim, *J. Power Sources.*, 166(2007) 92.
17. T. Springer, T. Zawodinski, S. Gottesfeld, *J. Electrochem. Soc.*, 138, (1999) 2334.
18. X. Yu, B. Zhou, A. Sobiesiak, *J. Power Sources.*, 147(2005) 184.
19. G. Wang, P. P. Mukherjee, C. Wang, *Electrochim. Acta*, 51 (2006) 3139.
20. C. M. Bautista-Rodríguez<sup>1</sup>, A. Rosas-Paletta, J. A. Rivera-Márquez<sup>1</sup>, O. Solorza-Feria, *Int. J. Electrochem. Sci.*, 4 (2009) 60.
21. Q. Wang, M. Eikerling, D. Song, Z. Liu, T. Navessin, Z. Xie, S. Holdcroft, *J. Electrochem. Soc.*, 151 (2004) A950.